Electronic Supplementary Material (ESI) for ChemComm.

Supporting Information

Tunable Microstructures of Ultralong Organic Phosphorescence Materials

Kun Liu,[a] Kaiwei Huang,[a] Anqi Lv,[a] Wenpeng Ye,[a] Yijun Yang,[b] Kang Shen,[a] Jiahuan Zhi,[a] He Wang,[a] Renxiang Zhang,[a] Jiamin Wang,[a] Huili Ma,[a] Huifang Shi,[a] Wei Yao,*[a] Zhongfu An,*[a] and Wei Huang*[ac]

a. Key Laboratory of Flexible Electronics (KLOFE) & Institute of Advanced Materials (IAM), Jiangsu National Synergistic Innovation Center for Advanced Materials (SICAM), Nanjing Tech University (NanjingTech), 30 South Puzhu Road, Nanjing 211800, P.R. China. E-mail: iamwhuang@njtech.edu.cn, iamzfan@njtech.edu.cn, iamwyao@njtech.edu.cn

b. Key Laboratory of Luminescence and Optical Information, Ministry of Education, Department of Physics, School of Science, Beijing Jiaotong University, Beijing 100044, P.R. China.

c. Frontiers Science Center for Flexible Electronics (FSCFE), Shaanxi Institute of Flexible Electronics (SIFE) & Shaanxi Institute of Biomedical Materials and Engineering (SIBME), North western Polytechnical University (NPU), 127 West Youyi Road, Xi'an 710072 China. E-mail: iamwhuang@njtech.edu.cn

Contents

I. Experimental details

Materials

PDBCz was synthesized by ourselves according to the previous literature.[1] The trichloromethane (TCM), dichloromethane (DCM), N,N-Dimethylformamide (DMF) and ethanol (EtOH) were purchased from commercial sources without further treatment.

Preparation of the microstructures

Rh-MSs, He-MSs and Re-MSs: In a typical preparation of Rh-MSs, 100 μL DMF and 50μL DCM were added into 1 mL PDBCz (1 mM) in TCM. Then, we dropped 20 μL of mixed solution onto cleaned glass, which was placed in a sealed petri dish with EtOH environment. The evaporation of the mixed solvent induced the self-assembly of PDBCz molecules. Finally, Rh-MSs were obtained on the glass after two hours. Similarly, we prepared He-MSs and Re-MSs by using a solvent evaporation method. When added 100 μL DMF and 50 μL DCM into 1 mL PDBCz (5 mM) in TCM, we obtained He-MSs. In contrast, He-MSs could be constructed if 100 μL DMF and 50 μL DCM were added into 1 mL PDBCz (8 mM) solution.

The preparation of crystals

Fabrication of the rhomboid crystals: 5.66 mg PDBCz powder (1×10^{-5} M) was added into TCM (10 mL) and subjected to ultrasound for 5 min. Afterward, 1 mL DMF and 1 mL DCM were added into the nearly transparent solution and stood for 3 days at room temperature and the rhomboid crystals gradually formed.
Fabrication of the rectangular crystals: 5.66 mg PDBCz powder (1×10^{-5} M) was added into TCM (2 mL) and subjected to ultrasound for 20 min. Then, 200 μL DMF and 200 μL DCM were added into the nearly transparent solution and stood for 3 days at room temperature and the rectangular crystals were obtained.
Fabrication of the hexagonal crystals: 5.66 mg PDBCz powder (1×10^{-5} M) was added into TCM (1 mL) and subjected to ultrasound for 60 min until the solution was nearly transparent. Afterward, 100 μL DMF and 100 μL DCM were added into solution and stood for 3 days at room temperature and the hexagonal crystals gradually constructed.

Measurements

To measure the PL spectra of single microsheet, the sheet was excited locally with a 375 nm picosecond pulsed diode laser (A.L.S. GmbH, Pilas-37X, 40 MHz) focused down to the diffraction limit. The excitation laser was filtered with a 400 nm notch filter. The light was subsequently coupled to a grating spectrometer (Andor, KY328i-B2) and recorded by a thermal-electrically cooled time-resolved CCD (Andor, DH334T-18U-03). To measure the phosphorescence spectra of single microsheet, the sheet was excited locally with a 360 nm LD pumped all-solid-state UV laser (Changchun New Industries Optoelectronics Tech, UV-FN-360, 50 mW) focused down to the diffraction limit. The excitation laser was filtered with a 400 nm notch filter. The light was subsequently coupled to a grating spectrometer (Andor, KY328i-B2) and recorded by a thermal-electrically cooled time-resolved CCD (Andor, DH334T-18U-03) with a delay time of 2 ms. Steady-state fluorescence/phosphorescence spectra of crystals were measured using HITACHI F-4600. The phosphorescence spectra were collected with a delay time of 5 ms. The lifetimes and time-resolved emission spectra were carried out on Edinburgh FLSP920 fluorescence spectrophotometer equipped with a xenon arc lamp (Xe 900) and microsecond flash-lamp (μF900),

respectively. Photoluminescence quantum efficiency was collected on a Hamamatsu Absolute PL Quantum Yield Spectrometer C11347 under ambient condition. SEM images were obtained by a (JSM-7800F) scanning electron microscopy (SEM). Fluorescence images were recorded using a Nikon DS-Ri2 Microscope Camera. The excitation source is a mercury lamp (Nikon INTENSILIGHT C-HGFI) equipped with a band-pass filter (330-380 nm for UV light). X-ray crystallography was achieved using a Bruker SMART APEX-II CCD diffractometer with graphite monochromated Mo-Kα radiation. Powder X-ray diffraction (PXRD) patterns were measured on an X-ray diffractometer (RIGAKU, RINT-ULTIMA III) using Cu Kα radiation (λ = 1.54051 Å) under ambient conditions.

Computational details

Morphological prediction: The theoretical growth morphologies of Rh-MSs, Re-MSs and He-MSs were calculated, respectively, by using the Materials Studio software based on the attachment energy theory.[2] Their molecular configurations were firstly optimized based on the respective single-crystal structures using the Build Bonds. The calculations about morphology and energy were performed through the Forcite and Morphology modules of the Material Studio software.

Intermolecular interactions calculation: Intermolecular interactions of these three crystals were calculated by the reduced density gradient (RDG) analysis.[3] The analysis of RDG was carried out by Multiwfn 3.6[4] and was volume rendered by VMD 1.9.3[5] based on the crystal data of rhomboid crystal, rectangular crystal and hexagonal crystal.

Binding energy calculation: The binding energy between optimized PDBCz molecules was calculated at B3LYP/def2TZVP level by using Gaussian 09 software package.[6] It was conducted according to the following equation considering the Basis Set Superposition Error (BSSE) correction: $E_{int} = E_{tot} - (E_1 + E_2) + E_{bsse}$, where E_{int} is the interaction energy between the two molecules, E_1 and E_2 is the energy of single molecules and E_{bsse} are the energies of BEES correction.

The spin-orbit coupling (SOC) constants (*ξ*) calculation: For model systems, the PDBCz molecules were extracted from the crystal structure of Rh, Re and He, respectively. All of the involved excited states properties in Rh, Re and He at the (TD) B3LYP/6-31G* level are based on crystal geometry in Gaussian 09 package.[6] The SOC matrix elements between singlet and triplet excited states were calculated by Beijing Density Function (BDF) program.[7,8]

II. Schematic diagram for the preparation process

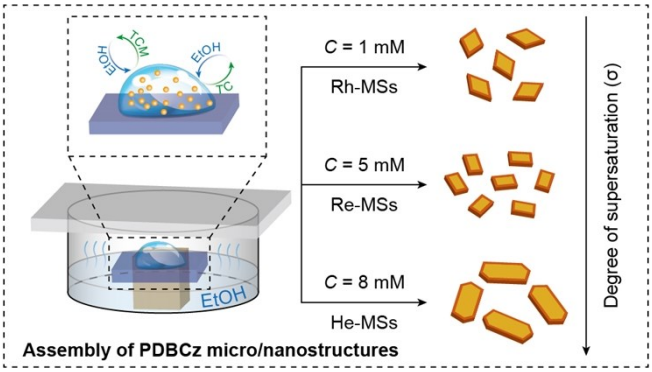

Figure S1. Schematic diagram for the preparation process of the PDBCz microstructures. The degree of supersaturation, $\sigma = C/C_0$ (C_0 is the equilibrium concentration), which could be assumed to be proportional to the solution concentration (C) at a constant temperature.

III. The concentration-dependent polymorph assembly process

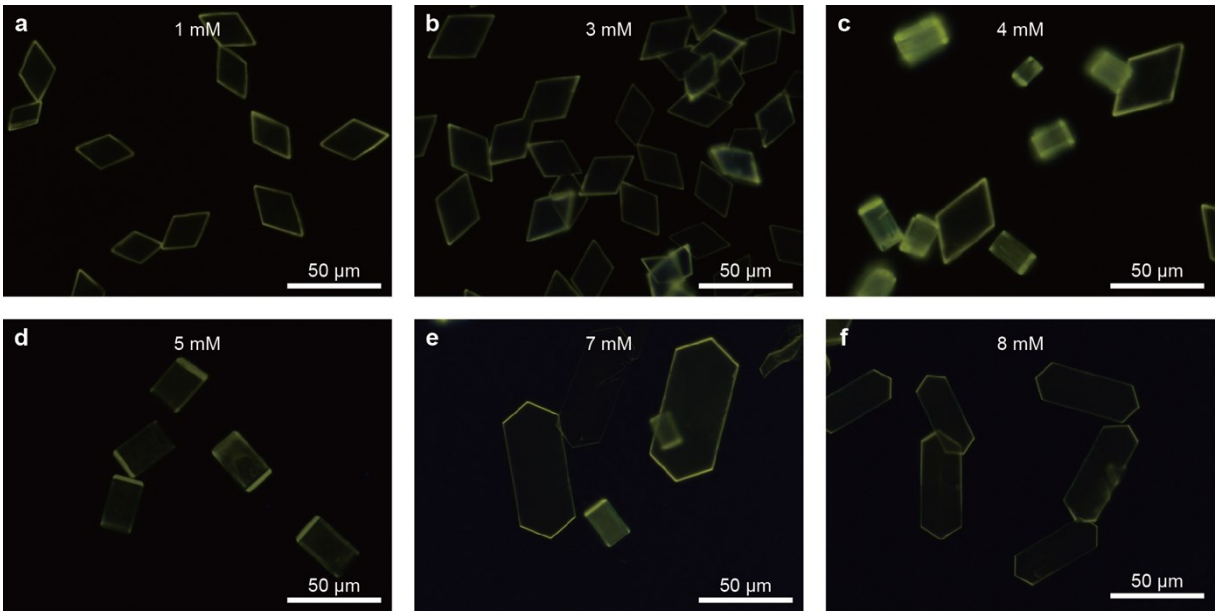

Figure S2. PL images for concentration-dependent self-assembled polymorphs with the PDBCz concentration of (a) 0.5 mM, (b) 1 mM, (c) 4 mM, (d) 5 mM, (e) 7 mM, and (f) 8 mM.

It can be seen that PDBCz molecular concentration are very critical for controlled synthesis of specific polymorphs. The low PDBCz molecular concentration (1 mM) only initiated the formation of the Rh-MSs. With the increasing of the PDBCz solution concentration, the Rh-MSs would gradually disappear, and next the Re-MSs started to appear and enlarge. When the concentration of PDBCz was further increased, the assembly of the He-MSs would be induced. The concentration-dependent polymorph assembly may be attributed to the supersaturation-controlled kinetically growth process.

IV Single crystal data

Table S1. Single-crystal data of the rhomboid crystals, rectangular crystals and hexagonal crystals.

Compound	rhomboid crystals	rectangular crystals	hexagonal crystals
Formula	$C_{30}H_{18}Br_2N_2$	$C_{30}H_{18}Br_2N_2$	$C_{30}H_{18}Br_2N_2$
Crystal system	monoclinic	monoclinic	monoclinic
Space group	$P2_1/c$	$P2_1/n$	$P2_1/n$
Cell Lengths (Å)	*a* 8.710(3)	*a* 8.462(3)	*a* 8.4373(15)
	b 17.149(5)	*b* 8.889(3)	*b* 8.8696(18)
	c 8.657(3)	*c* 15.712(5)	*c* 15.702(3)
Cell Angeles (°)	*α* 90	*α* 90	*α* 90
	β 116.339	*β* 99.317	*β* 99.385
	γ 90	*γ* 90	*γ* 90
Z	2	2	2
R-factor (%)	4.09	4.44	3.98
CCDC number	2061463	2061462	2061461

Table S2. Bond lengths (Å) of PDBCz in rhomboid crystals.

Parameter	Bond lengths/ Å
Br(1)-C(14)	1.887(3)
C(1)-C(2)	1.373(5)
C(1)-N(1)	1.406(4)
C(1)-C(6)	1.409(4)
C(2)-C(3)	1.382(6)
C(2)-H(2)	0.93
C(3)-C(4)	1.389(6)
C(3)-H(3)	0.93
C(4)-C(5)	1.379(6)
C(4)-H(4)	0.93
C(5)-C(6)	1.412(5)
C(5)-H(5)	0.93
C(6)-C(7)	1.437(5)
C(7)-C(8)	1.394(5)

C(7)-C(12)	1.420(5)
C(8)-C(9)	1.377(6)
C(8)-H(8)	0.93
C(9)-C(10)	1.388(6)
C(9)-H(9)	0.93
C(10)-C(11)	1.379(5)
C(10)-H(10)	0.93
C(11)-C(12)	1.382(5)
C(11)-H(11)	0.93
C(12)-N(1)	1.386(4)
C(13)-C(15)#1	1.387(4)
C(13)-C(14)	1.395(4)
C(13)-N(1)	1.431(3)
C(14)-C(15)	1.381(4)
C(15)-C(13)#1	1.387(4)
C(15)-H(15)	0.93

Table S3. Angles (°) of PDBCz in rhomboid crystals.

Parameter	Angles/ °
C(2)-C(1)-N(1)	128.8(3)
C(2)-C(1)-C(6)	123.0(3)
N(1)-C(1)-C(6)	108.2(3)
C(1)-C(2)-C(3)	117.1(3)
C(1)-C(2)-H(2)	121.4
C(3)-C(2)-H(2)	121.4
C(2)-C(3)-C(4)	122.5(4)
C(2)-C(3)-H(3)	118.8

C(4)-C(3)-H(3)	118.8
C(5)-C(4)-C(3)	119.9(4)
C(5)-C(4)-H(4)	120.1
C(3)-C(4)-H(4)	120.1
C(4)-C(5)-C(6)	119.6(4)
C(4)-C(5)-H(5)	120.2
C(6)-C(5)-H(5)	120.2
C(1)-C(6)-C(5)	117.9(3)
C(1)-C(6)-C(7)	107.4(3)
C(5)-C(6)-C(7)	134.7(3)
C(8)-C(7)-C(12)	118.6(3)
C(8)-C(7)-C(6)	134.4(3)
C(12)-C(7)-C(6)	107.0(3)
C(9)-C(8)-C(7)	119.1(3)
C(9)-C(8)-H(8)	120.5
C(7)-C(8)-H(8)	120.5
C(8)-C(9)-C(10)	121.1(3)
C(8)-C(9)-H(9)	119.4
C(10)-C(9)-H(9)	119.4
C(11)-C(10)-C(9)	121.7(4)
C(11)-C(10)-H(10)	119.2
C(9)-C(10)-H(10)	119.2

Table S4. Bond lengths (Å) of PDBCz in rectangular crystals.

Parameter	Bond lengths/ Å
Br(1)-C(14)	1.888(2)
C(1)-C(2)	1.377(4)

C(1)-N(1)	1.393(3)
C(1)-C(6)	1.417(4)
C(2)-C(3)	1.388(5)
C(2)-H(2)	0.93
C(3)-C(4)	1.393(5)
C(3)-H(3)	0.93
C(4)-C(5)	1.379(5)
C(4)-H(4)	0.93
C(5)-C(6)	1.389(4)
C(5)-H(5)	0.93
C(6)-C(7)	1.445(5)
C(7)-C(8)	1.406(4)
C(7)-C(12)	1.412(4)
C(8)-C(9)	1.378(6)
C(8)-H(8)	0.93
C(9)-C(10)	1.391(5)
C(9)-H(9)	0.93
C(10)-C(11)	1.387(4)
C(10)-H(10)	0.93
C(11)-C(12)	1.381(4)
C(11)-H(11)	0.93
C(12)-N(1)	1.401(3)
C(13)-C(14)	1.383(4)
C(13)-C(15)#1	1.390(3)
C(13)-N(1)	1.422(3)
C(14)-C(15)	1.383(3)
C(15)-C(13)#1	1.390(3)

C(15)-H(15)	0.93

Table S5. Angles (°) of PDBCz in rectangular crystals.

Parameter	Angles/ °
C(2)-C(1)-N(1)	129.6(2)
C(2)-C(1)-C(6)	122.2(3)
N(1)-C(1)-C(6)	108.1(2)
C(1)-C(2)-C(3)	117.7(3)
C(1)-C(2)-H(2)	121.2
C(3)-C(2)-H(2)	121.2
C(2)-C(3)-C(4)	120.9(3)
C(2)-C(3)-H(3)	119.5
C(4)-C(3)-H(3)	119.5
C(5)-C(4)-C(3)	121.1(3)
C(5)-C(4)-H(4)	119.4
C(3)-C(4)-H(4)	119.4
C(4)-C(5)-C(6)	119.2(3)
C(4)-C(5)-H(5)	120.4
C(6)-C(5)-H(5)	120.4
C(5)-C(6)-C(1)	118.8(3)
C(5)-C(6)-C(7)	133.9(3)
C(1)-C(6)-C(7)	107.3(2)
C(8)-C(7)-C(12)	118.0(3)
C(8)-C(7)-C(6)	134.9(3)
C(12)-C(7)-C(6)	107.0(2)
C(9)-C(8)-C(7)	119.2(3)
C(9)-C(8)-H(8)	120.4

C(7)-C(8)-H(8)	120.4
C(8)-C(9)-C(10)	121.1(3)
C(8)-C(9)-H(9)	119.4
C(10)-C(9)-H(9)	119.4
C(11)-C(10)-C(9)	121.5(3)
C(11)-C(10)-H(10)	119.3
C(9)-C(10)-H(10)	119.3

Table S6. Bond lengths (Å) of PDBCz in hexagonal crystals.

Parameter	Bond lengths/ Å
Br(1)-C(15)	1.883(3)
C(1)-C(2)	1.377(5)
C(1)-N(1)	1.395(4)
C(1)-C(6)	1.410(4)
C(2)-C(3)	1.385(5)
C(2)-H(2)	0.93
C(3)-C(4)	1.389(6)
C(3)-H(3)	0.93
C(4)-C(5)	1.364(6)
C(4)-H(4)	0.93
C(5)-C(6)	1.402(5)
C(5)-H(5)	0.93
C(6)-C(7)	1.431(5)
C(7)-C(8)	1.392(5)
C(7)-C(12)	1.415(4)
C(8)-C(9)	1.374(6)
C(8)-H(8)	0.93

C(9)-C(10)	1.389(6)
C(9)-H(9)	0.93
C(10)-C(11)	1.392(5)
C(10)-H(10)	0.93
C(11)-C(12)	1.369(5)
C(11)-H(11)	0.93
C(12)-N(1)	1.393(4)
C(13)-C(14)	1.377(4)
C(13)-C(15)#1	1.386(4)
C(13)-N(1)	1.420(4)
C(14)-C(15)	1.380(4)
C(14)-H(14)	0.93
C(15)-C(13)#1	1.386(4)

Table S7. Angles (°) of PDBCz in hexagonal crystals.

Parameter	Angles/ °
C(2)-C(1)-N(1)	128.5(3)
C(2)-C(1)-C(6)	123.1(3)
N(1)-C(1)-C(6)	108.4(3)
C(1)-C(2)-C(3)	116.9(3)
C(1)-C(2)-H(2)	121.5
C(3)-C(2)-H(2)	121.5
C(2)-C(3)-C(4)	121.3(4)
C(2)-C(3)-H(3)	119.3
C(4)-C(3)-H(3)	119.3
C(5)-C(4)-C(3)	121.4(3)
C(5)-C(4)-H(4)	119.3

C(3)-C(4)-H(4)	119.3
C(4)-C(5)-C(6)	119.3(3)
C(4)-C(5)-H(5)	120.3
C(6)-C(5)-H(5)	120.3
C(5)-C(6)-C(1)	117.9(3)
C(5)-C(6)-C(7)	135.1(3)
C(1)-C(6)-C(7)	107.0(3)
C(8)-C(7)-C(12)	118.2(3)
C(8)-C(7)-C(6)	134.2(3)
C(12)-C(7)-C(6)	107.6(3)
C(9)-C(8)-C(7)	119.4(3)
C(9)-C(8)-H(8)	120.3
C(7)-C(8)-H(8)	120.3
C(8)-C(9)-C(10)	121.3(4)
C(8)-C(9)-H(9)	119.4
C(10)-C(9)-H(9)	119.4
C(9)-C(10)-C(11)	120.8(4)
C(9)-C(10)-H(10)	119.6
C(11)-C(10)-H(10)	119.6

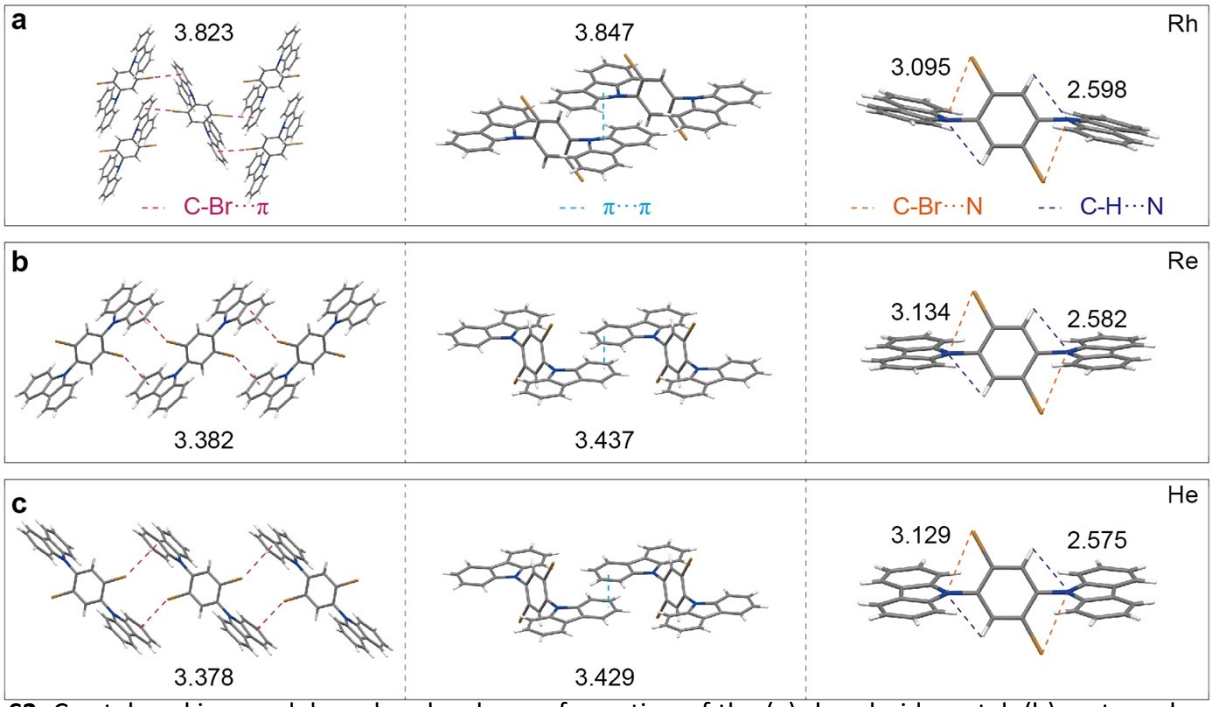

Figure S3. Crystal packing models and molecular conformation of the (a) rhomboid crystal, (b) rectangular crystal and (c) hexagonal crystal.

In rhomboid crystal, the distance of [C–Br···π] halogen bonding between bromine atom and carbazyl group is 3.823 Å, which connect the PDBCz molecule with four surrounding molecules. Moreover, there is a large overlap on the carbazyl group with formed π···π stacking (3.847 Å) for a pair of PDBCz molecules in this crystal. In rectangular crystal, each PDBCz molecule in the crystal is connected with two surrounding molecules through [C–Br···π] halogen bonding between bromine atom and carbazyl group with distance of 3.382 Å, and the distance of π···π stacking is 3.437 Å for a pair of PDBCz molecules. The molecular packing arrangements of hexagonal crystal are the same as the Re-MSs while the distance of [C–Br···π] halogen bonding and π···π stacking are 3.378 Å and 3.429 Å, respectively. The different packing models of crystals might be caused by the different molecular conformations of PDBCz, which lead to different inter- / intramolecular interactions. Both three crystals existed two types of intramolecular interactions, including C–Br···N and C–H···N. For rhomboid crystal, the distance of C–Br···N bonding is 3.095 Å, which is smaller than that of rectangular crystal (3.134 Å) and hexagonal crystal (3.129 Å). The distance of C–H···N bonding in three crystals, however, are nearly the same. For rhomboid crystal, the distance of C–H···N bonding is 2.598 Å, while the distance of C–H···N bonding for rectangular crystal and hexagonal crystal are 2.582 Å and 2.575 Å, respectively.

Table S8. Calculated attachment energies of different crystal faces for (a) Rh-MSs and (b) Re-MSs and (c) He-MSs, respectively, using the Material Studio package.

a	**hkl**	d_{hkl}**/Å**	E_{att}**(Total)/kcal·mol^{-1}**	**% Total facet area**
	(020)	8.57	-36.14	45.65
	(100)	7.80	-67.02	27.59
	(110)	7.10	-77.46	
	(011)	7.07	-76.55	26.76

b	hkl	d_{hkl}/Å	E_{att}(Total)/kcal·mol^{-1}	% Total facet area
	(10-1)	7.90	-75.56	18.07
	(002)	7.75	-57.33	19.30
	(011)	7.71	-60.24	45.36
	(101)	6.90	-69.53	17.27

c	hkl	d_{hkl}/Å	E_{att}(Total)/kcal·mol^{-1}	% Total facet area
	(10-1)	7.89	-76.02	13.81
	(002)	7.74	-57.64	20.94
	(011)	7.70	-60.55	38.38
	(101)	6.88	-69.99	13.22
	(110)	6.07	-76.77	13.64

The attachment energy (E_{att}) is defined as the energy released on the addition of a growth slice to the surface of a growing crystal. Thus, the growth rate of the crystal face could be assumed to be proportional to its attachment energy by a layer-by-layer mechanism.[9] That is, the surfaces with attachment energies smaller in magnitude have lower growth rates and will be morphologically important. For Rh-MSs, the smallest attachment energies in magnitude obtained from the (020) face suggest that it has the slowest growth rates and will be more present in the final crystal morphology. In contrast, the (002) face in Re-MSs and He-MSs is the preferred growth face due to the lowest attachment energies in magnitude.

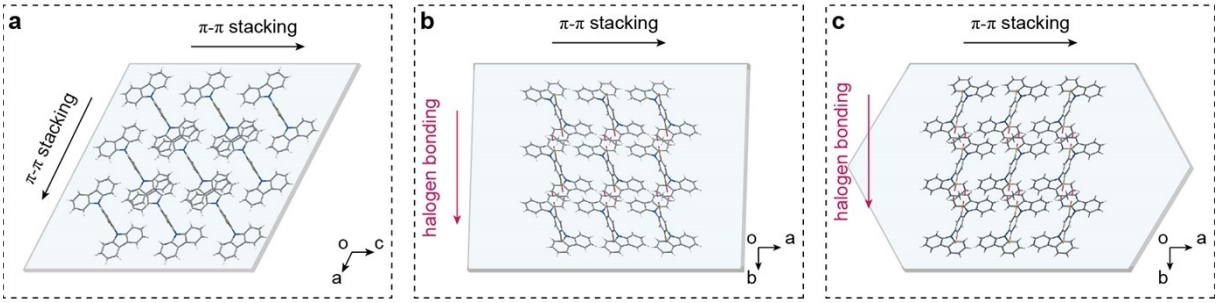

Figure S4. (a) The packing arrangement of Rh-MSs when viewed perpendicular to the *b* axis. (b) The packing arrangement of Re-MSs when viewed perpendicular to the *c* axis. (c) The packing arrangement of He-MSs when viewed perpendicular to the *c* axis.

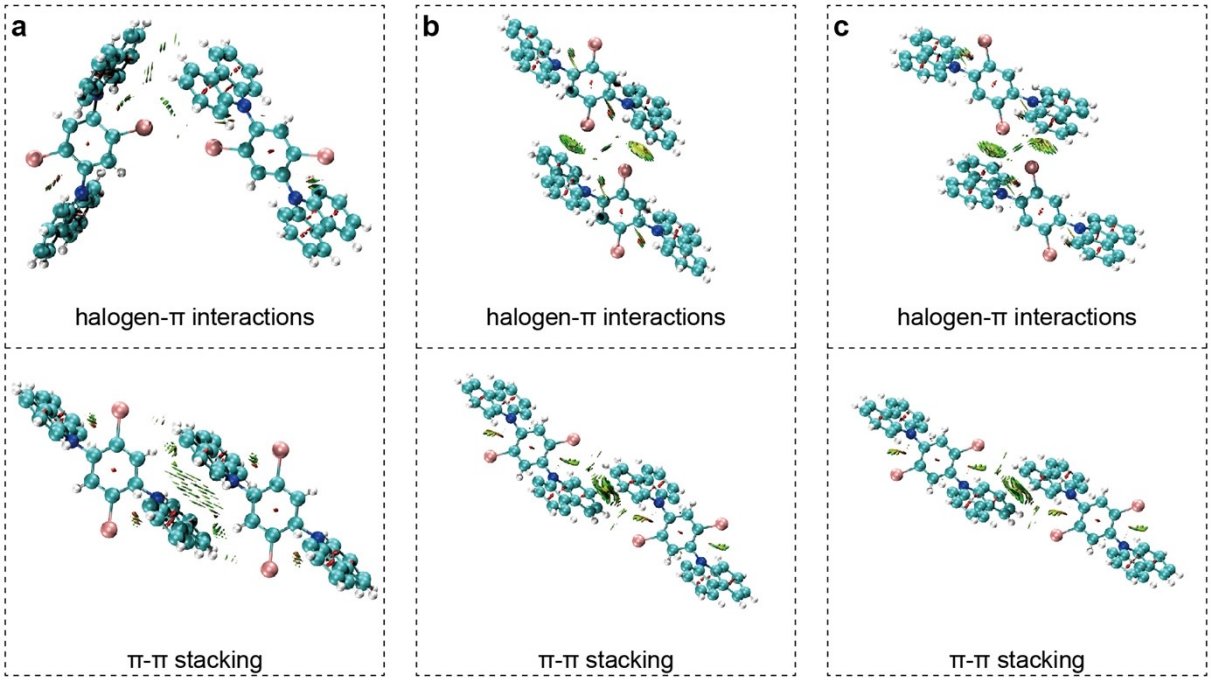

Figure S5. The calculated intermolecular weak interactions (green isosurface) in dimers of the (a) rhomboid crystal, (b) rectangular crystal and (c) hexagonal crystal (the isovalue is 0.005).

In order to make sure that the halogen-π interactions and π-π stacking are proposed as the driving forces for packing and which one is stronger/weaker, we performed a RDG analysis to directly show the intermolecular weak interactions. As shown in Figure S5, the isosurface between two carbazole units in rhomboid crystal was more obvious when compared with the isosurface between carbazole unit and bromine atom. This means that the π-π stacking in rhomboid crystal is stronger than the halogen-π interactions and is proposed as the driving forces for packing. As for the rectangular crystal and hexagonal crystal, the isosurface between two carbazole units is almost the same as the isosurface between carbazole and bromine atom. This result suggests that in rectangular and hexagonal crystals, the magnitude of the π-π stacking and the halogen bond interactions are close, which means that both of them are proposed as the driving forces for packing.

Table S9. Calculation results of binding energies for rhomboid crystal, rectangular crystal and hexagonal crystal, performed by Gaussian 09 software package.

Crystal	binding energies (kcal/mol)	
	halogen-π interactions	π-π interactions
Rhomboid	-25.489	-28.818
Rectangular	-23.898	-23.999
Hexagonal	-23.910	-23.985

In order to compare the interaction energies quantitatively, we calculated the binding energies of these three crystals. As shown in Table S9, the binding energy of π-π interactions in rhomboid crystal is larger than that of halogen-π interactions. As for the rectangular crystal and hexagonal crystal, the binding energies of π-π interactions are close to the halogen-π interactions. The results of binding energies calculation are consistent with the trend indicated by RDG analysis.

Table S10. Calculated surface energies of different crystal faces for (a) Rh-MSs and (b) Re-MSs and (c) He-MSs, respectively, using the Material Studio package.

a	**hkl**	d_{hkl}/Å	E_{surf}/kcal·mol^{-1}	**% Total facet area**
	(020)	8.57	0.1338	39.64
	(100)	7.80	0.2294	21.35
	(110)	7.10	0.2484	8.13
	(011)	7.07	0.2389	30.88

b	**hkl**	d_{hkl}/Å	E_{surf}/kcal·mol^{-1}	**% Total facet area**
	(10-1)	7.90	0.2594	14.86
	(002)	7.75	0.1922	18.63
	(011)	7.71	0.2024	44.27
	(101)	6.90	0.2086	22.24

c	**hkl**	d_{hkl}/Å	E_{surf}/kcal·mol^{-1}	**% Total facet area**
	(10-1)	7.89	0.2620	9.68
	(002)	7.74	0.1942	21.04
	(011)	7.70	0.2043	33.53
	(101)	6.88	0.2106	14.78
	(110)	6.07	0.2296	20.96

The total surface energy ($E_{surf\text{-}total}$) is calculated by the sum up of surface energy of each single crystal surface through multiplying the surface area and surface energy. The $E_{surf\text{-}total}$ of Rh-MSs, Re-MSs and He-MSs is calculated to be 0.1960 kcal.mol^{-1}, 0.2103 kcal.mol^{-1} and 0.2140 kcal.mol^{-1}, respectively.

Table S11. Calculation results of lattice energies for Rh-MSs, Re-MSs and He-MSs, performed by Materials Studio package.

	Lattice energy (kcal/mol)	**Van der Waal contribution (kcal/mol)**	**Electrostatic contribution (kcal/mol)**	**Molecular number per unit cell**
Rh-MSs	-115.483	-115.483	0	2
Re-MSs	-112.690	-112.690	0	1
He-MSs	-113.319	-113.319	0	1

The lattice energy of Rh-MSs calculate by Materials Studio is -115.483 kcal/mol with two molecules per unit cell, while the lattice energy of Re-MSs is -112.690 kcal/mol with one molecules per unit cell. This means that the Gibbs energy of the Re-MSs is 112.69 − 115.483 ÷ 2 = 54.9485 kcal lower than the Rh-MSs every mol of molecules. That is, the Re-MSs should be more thermodynamically stable than the Rh-MSs.

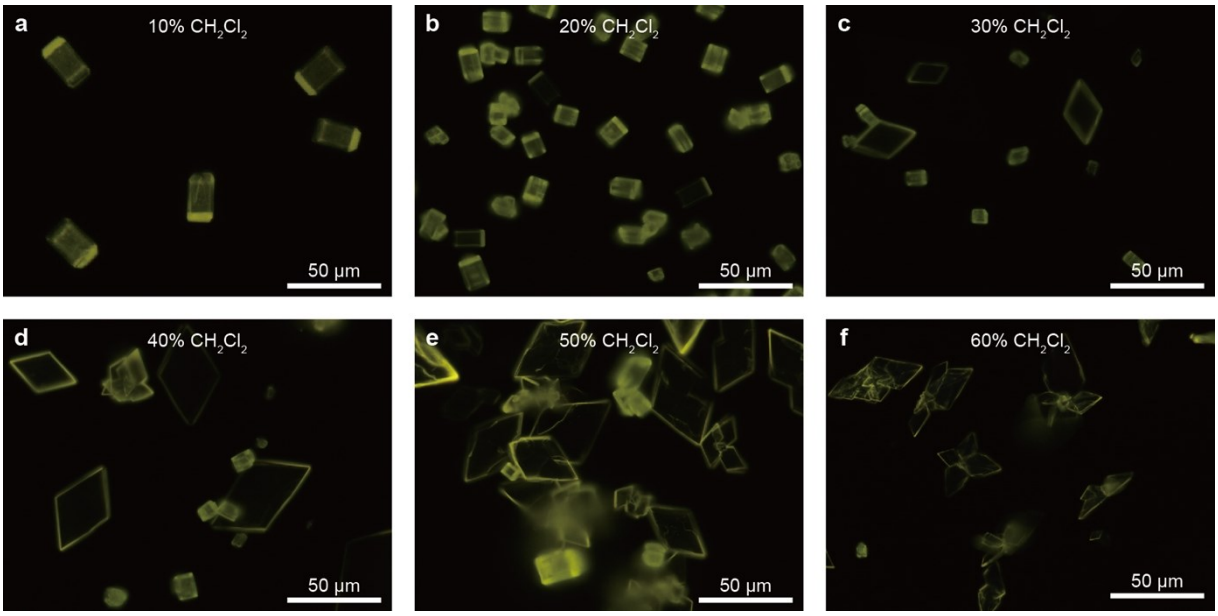

Figure S6. PL images for solvent-ratio-dependent self-assembled PDBCz crystals with the CH_2Cl_2 volume fraction of (a) 10%, (b) 20%, (c) 30%, (d) 40%, (e) 50%, and (f) 60% in the CH_2Cl_2/CH_3Cl mixture, where the PDBCz (5 mM) concentration remains unchanged.

By adding a lower boiling solvent (CH_2Cl_2) into the CH_3Cl, the kinetic assembly rate could be well modulated. Under the low CH_2Cl_2 fractions, the speed of solvent evaporation and self-assembly is relatively slow, so thermodynamic factors (high PDBCz concentration) dominate the self-assembly process, and the final product will be the more thermodynamically stable crystal form (i.e., Re-MSs). With the increasing of the CH_2Cl_2 fraction, the crystal morphology of Re-MSs began to gradually irregular, and a certain amount of Rh-MSs appeared. When the CH_2Cl_2 fraction reaches more than 50%, the solvent evaporation and self-assembly speed are very fast, so that the kinetic factor (evaporation rate) dominates the self-assembly process. The final product would be the kinetically stable crystal form (i.e., Rh-MSs), in which the shape is irregular rhombus-like sheet. Therefore, it can be preliminarily concluded that the Re-MSs is a more thermodynamically stable crystal form than the Rh-MSs.

V Additional photophysical properties of PDBCz in crystalline state

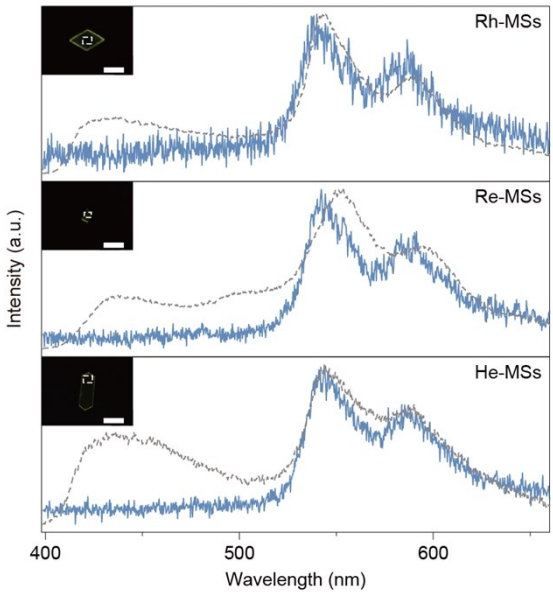

Figure S7. The Steady-state photoluminescence (black line) and phosphorescence spectra (red line) of Rh-MSs, Re-MSs and He-MSs, respectively. Insets: corresponding PL microscopy images. Scale bars are 25 μm.

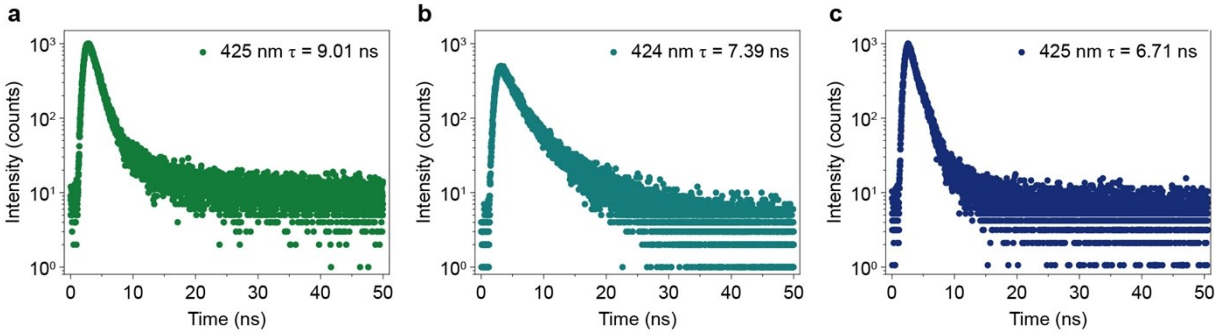

Figure S8. Lifetime decay profiles of the fluorescence emission bands of (a) rhomboid crystals, (b) rectangular crystals and (c) hexagonal crystals under ambient conditions.

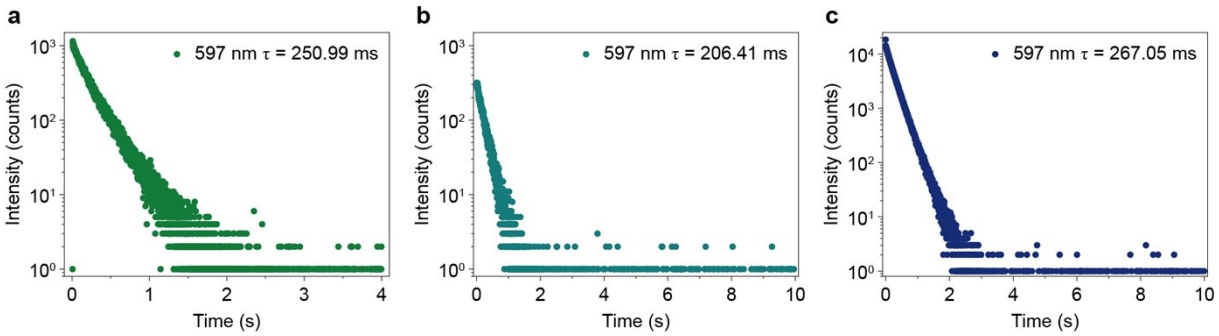

Figure S9. Lifetime decay profiles of the phosphorescence emission bands at 597 nm of (a) rhomboid crystals, (b) rectangular crystals and (c) hexagonal crystals under ambient conditions.

Table S12. Phosphorescence lifetimes (τ) and its percentage of rhomboid crystals, rectangular crystals and hexagonal crystals[a].

Crystal	**Phosphorescence**				
	Wavelength (nm)	τ_1 (ms)	A_1 (%)	τ_2 (ms)	A_2 (%)
Rhomboid	550	123.66	24.49	263.31	75.51
	597	96.08	16.64	250.99	83.86
Rectangular	550	209.40	100		
	597	206.41	100		
Hexagonal	550	158.55	26.53	269.14	73.47
	597	153.67	25.38	267.05	74.62

[a] Determined from the fitting function of $I(t) = A_1 e^{-t/\tau 1} + A_2 e^{-t/\tau 2}$.

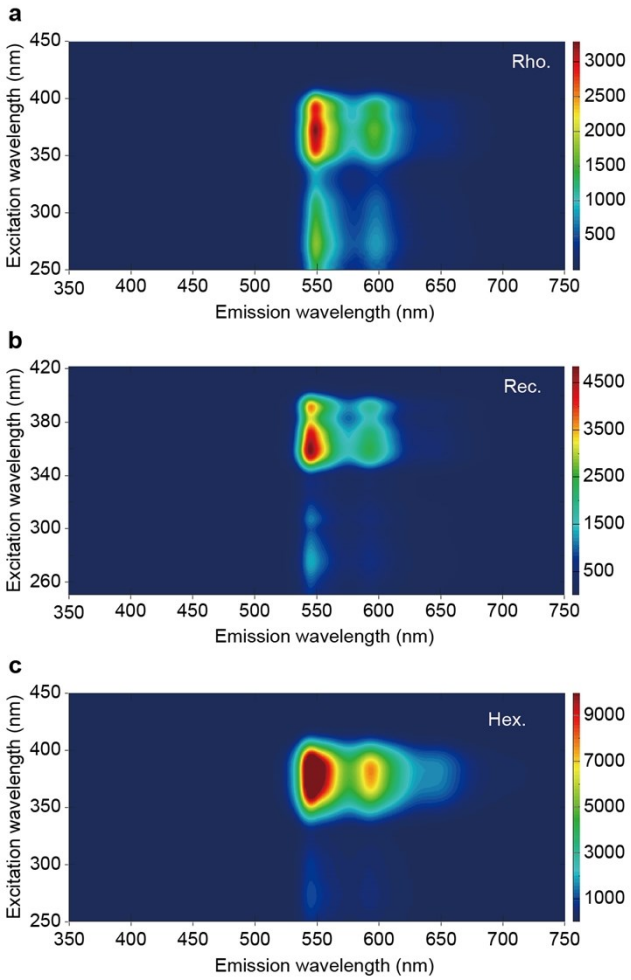

Figure S10. Excitation-phosphorescence mapping of (a) rhomboid crystals, (b) rectangular crystals and (c) hexagonal crystals.

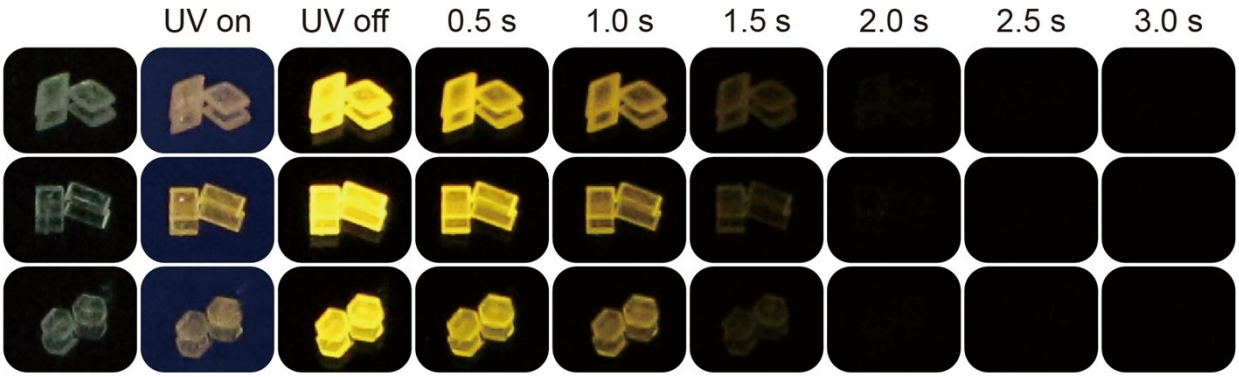

Figure S11. The photographs of rhomboid, rectangular and hexagonal crystals monitoring the deactivation process of UOP excited at 365 nm UV lamp (40 mW/cm^2) under ambient conditions, respectively.

VI. Theoretical calculations

Calculation of rate parameters: The radiative and non-radiative rate constants were calculated using the following equations.

It's considered that the Φ_{IC} is approximately equal to zero when the S_1–S_0 energy gaps($\Delta E_{S1\rightarrow S0}$) for materials are greater than 2.17 eV.[10-12] In this work, both $\Delta E_{S1\rightarrow S0}$ for rhomboid, rectangular and hexagonal crystals are 2.92 eV, calculated by the equation $\Delta E_{S1\rightarrow S0} = 1240/\lambda$.

$$k_r^{Fluo} = \Phi_{Fluo} / \tau_{Fluo} \quad \text{(a)}$$

$$\Phi_{isc} = 1 - \Phi_{Fluo} - \Phi_{ic} \approx 1 - \Phi_{Fluo} \quad \text{(b)}$$

$$\tau_{Fluo} = \frac{1}{k_r^{Fluo} + k_{nr}^{Fluo} + k_{isc}};$$

$$\Phi_{isc} = \frac{k_{isc}}{k_r^{Fluo} + k_{nr}^{Fluo} + k_{isc}} = k_{isc} \times \tau_{Fluo};$$

$$k_{isc} = \frac{\Phi_{isc}}{\tau_{Fluo}} \quad \text{(c)}$$

$$\tau_{Phos} = \frac{1}{k_r^{Phos} + k_{nr}^{Phos}};$$

$$\Phi_{Phos} = \frac{\Phi_{isc} \times k_r^{Phos}}{k_r^{Phos} + k_{nr}^{Phos}} = \Phi_{isc} \times k_r^{Phos} \times \tau_{Phos};$$

$$k_r^{Phos} = \frac{\Phi_{Phos}}{\Phi_{isc} \times \tau_{Phos}} \quad \text{(d)}$$

$$k_{nr}^{Phos} = \frac{1}{\tau_{Phos}} - k_r^{Phos} \quad \text{(e)}$$

Where, k_r^{Fluo}, k_{isc}, k_r^{Phos}, k_{nr}^{Phos} are the radiative rate constant of prompt fluorescence, rate constant of intersystem crossing (ISC), radiative rate constant of phosphorescence and nonradiative rate constant of phosphorescence.

Table S13. Dynamic photophysical parameters of ultralong organic phosphorescence.

Crystal	τ_F [ns]	Φ_F [%]	τ_P [ms]	Φ_P [%]	k_r^{Fluo} [s^{-1}][(a)]	Φ_{isc} [%] [(b)]	k_{isc} [s^{-1}][(c)]	k_r^{phos} [s^{-1}][(d)]	k_{nr}^{phos} [s^{-1}][(e)]
Rhomboid	9.01	1.78	263.31	19.12	1.98×10^6	98.22	1.09×10^8	0.74	3.06
Rectangular	7.39	5.52	209.40	31.68	7.47×10^6	94.48	1.28×10^8	1.60	3.18
Hexagonal	6.71	2.15	269.14	32.95	3.20×10^6	97.85	1.46×10^8	1.25	2.47

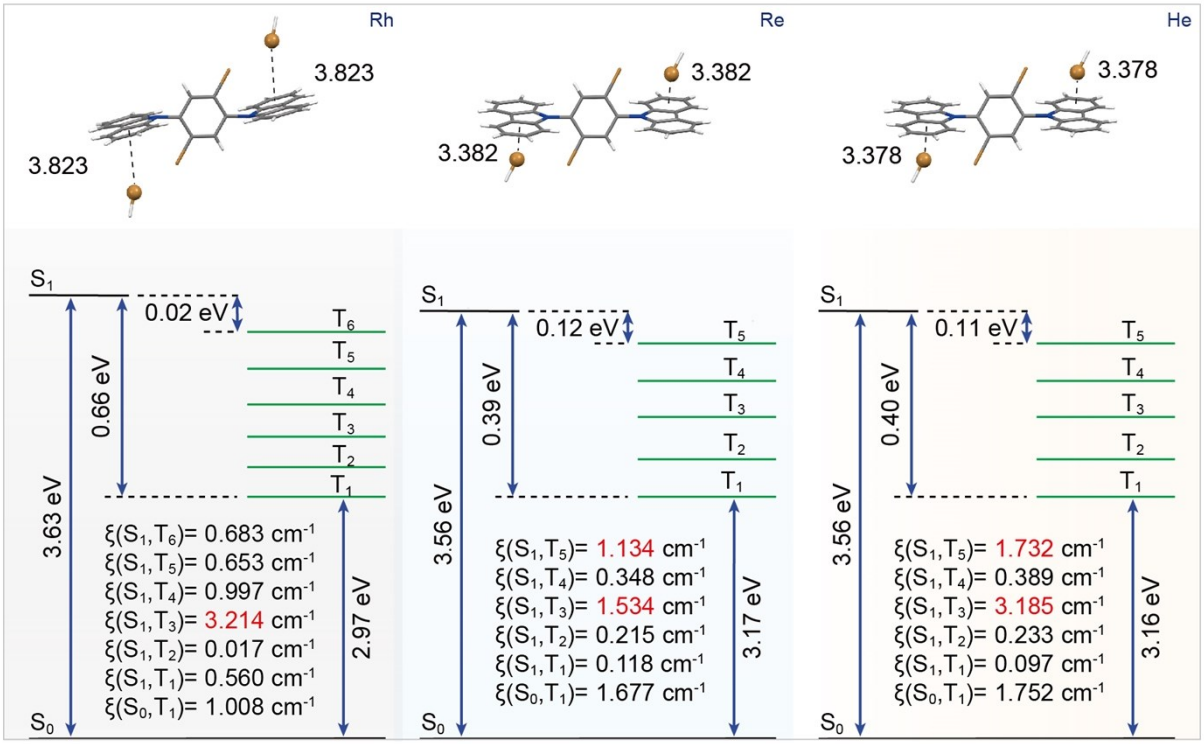

Figure S12. The model selected as calculated SOC constant, calculated energy diagram and SOC (ξ) of rhomboid crystals, rectangular crystals and hexagonal crystals, respectively with external heavy atoms effect.

VII. References

1 H. Shi, L. Song, H. Ma, C. Sun, K. Huang, A. Lv, W. Ye, H. Wang, S. Cai, W. Yao, Y. Zhang, R. Zheng, Z. An and W. Huang, *J. Phys. Chem. Lett.*, 2019, **10**, 595-600.
2 D. Winn, M. F. Doherty, *AIChE J.,* 2000, **46**, 1348-1367.
3 E. R. Johnson, S. Keinan, P. Mori-Sánchez, J. Contreras-García, A. J. Cohen, W. Yang, *J. Am. Chem. Soc.,* 2010, **132**, 6498–6506.
4 T. Lu, F. Chen, *J. Comput. Chem.*, 2012, **33**, 580-592.
5 W. Humphrey, A. Dalke, K. Schulten, *J. Mol. Graph. Model.,* 1996, **14**, 33-38.
6 M. J. Frisch, G. W. Trucks, H. B. Schlegel, G. E. Scuseria, M. A. Robb, J. R. Cheeseman, G. Scalmani, V. Barone, B. Mennucci, G. A. Petersson, H. Nakatsuji, M. Caricato, X. Li, H. P. Hratchian, A. F. Izmaylov, J. Bloino, G. Zheng, J. L. Sonnenberg, M. Hada, M. Ehara, K. Toyota, R. Fukuda, J. Hasegawa, M. Ishida, T. Nakajima, Y. Honda, O. Kitao, H. Nakai, T. Vreven, J. A. Montgomery. Jr., J. E. Peralta, F. Ogliaro, M. J. Bearpark, J. Heyd, E. N. Brothers, K. N. Kudin, V. N. Staroverov, R. Kobayashi, J. Normand, K. Raghavachari, A. P. Rendell, J. C. Burant, S. S. Iyengar, J. Tomasi, M. Cossi, N. Rega, N. J. Millam, M. Klene, J. E. Knox, J. B. Cross, V. Bakken, C. Adamo, J. Jaramillo, R. Gomperts, R. E. Stratmann, O. Yazyev, A. J. Austin, R. Cammi, C. Pomelli, J. W. Ochterski, R. L. Martin, K. Morokuma, V. G. Zakrzewski, G. A. Voth, P. Salvador, J. J. Dannenberg, S. Dapprich, A. D. Daniels, Farkas, J. B. Foresman, J. V. Ortiz, J. Cioslowski, D. J. Fox. Gaussian 09 revison C.01; Gaussian, Inc.: Wallingford, CT, 2009.
7 W. Liu, F. Wang and L. Li, *J. Theor. Comput. Chem*., 2003, **2**, 257-272.
8 W. Liu, G. Hong, D. Dai, L. Li and M. Dolg, *Theor. Chem. Acc*., 1997, **96**, 75-83.
9 P. Hartman, P. Bennema, *J. Cryst. Growth,* 1980, **49**, 145-146.
10 S. Hirata, *Adv. Sci.,* 2019, **2**, 1900410.
11 S. Hirata, *Adv. Optical Mater.,* 2017, **5**, 1700116.
12 J. N. Turro, *Modern Molecular Photochemistry*, University Science Books, Sausalito, CA, 1991, p. 178.